PHYSICAL REVIEW C

NUCLEAR PHYSICS

THIRD SERIES, VOL. 1, NO. 4 APRIL 1970

Analysis of Proton Elastic Scattering Using Potentials Derived from Nucleon-Density Distributions and Two-Body Potentials*

G. W. GREENLEES, W. MAKOFSKE, AND G. J. PYLE†

Department of Physics, University of Minnesota, Minneapolis, Minnesota 55455

(Received 8 October 1969)

Proton elastic scattering data at 30.3 MeV are analyzed using the optical model recently developed by Greenlees, Pyle, and Tang. The present analysis differs from that given in the original paper in using a model-exact treatment of the spin-orbit and isospin terms of the potential. The quality of the fits obtained is insensitive to the detailed manner in which the potential is constructed and, in particular, to the choice of nucleon–nucleon force parameters. These parameters are therefore taken from an analysis of low-energy nucleon-nucleon scattering data, thus enabling the present analysis to give nuclear-neutron rms radii. The n-p rms-radius difference is about zero for medium-weight elements and 0.1–0.2 F for heavy elements. Evidence is presented supporting the conclusion that the volume integral and the rms radius of the real central potential are the well-defined quantities which can be deduced from analyses of elastic proton scattering data.

I. INTRODUCTION

IN a recent paper, Greenlees, Pyle, and Tang[1] developed an optical model in which the real parts of the potential were derived from nuclear-matter distributions and the nucleon-nucleon force. When applied to proton elastic scattering data at 14.5, 30.3, and 40 MeV, the model was able to fit the data as well as standard optical-model treatments, despite having fewer adjustable parameters. One of the findings of this analysis was that, although the individual geometrical parameters could take a wide range of values, the rms radius of the real central potential was well defined and independent of the incident energy. For a given range of the two-body force, values for the nuclear rms matter radii could be obtained. These values were greater than the corresponding rms proton radii, derived from electron scattering and muonic x-ray work, and implied that the nuclear-neutron rms radii were greater than the nuclear-proton rms radii by about 0.6 F for all nuclei considered when a Yukawa two-body force of ms radius 2.25 F[2] was used.

Although the model, as developed in Ref. 1, gives a first-order treatment of the problem, the actual analysis of data reported there involved two additional assumptions in the calculation of the isospin and spin-orbit terms. In the present analysis, these approximations have been removed and proton data at 30.3 MeV analyzed using the complete model. It is found that the neutron-proton rms-radii differences are reduced by 0.1–0.2 F for a Yukawa two-body force of ms radius 2.25 F[2]. However, the fits to the data are found to be relatively insensitive to both the magnitude of the isospin term and the range of the direct part of the nucleon-nucleon force. When these quantities are chosen to agree with a recent analysis of low-energy nucleon-nucleon data, which used a Gaussian shape, a further reduction is effected in the nuclear neutron-proton rms-radius differences to values around zero for medium-weight elements and 0.1–0.2 F for heavy elements.

Confirmation is provided that the volume integral and the rms radius of the real central potential are well-defined quantities which can be extracted from elastic scattering data as was suggested in Ref. 1 and by Becchetti and Greenlees.[2] This result is insensitive to the detailed form of the potential used.

* Work supported in part by the Atomic Energy Commission.

† Present address: Department of Physics, University of Birmingham, England.

[1] G. W. Greenlees, G. J. Pyle, and Y. C. Tang, Phys. Rev. **171**, 1115 (1968).

[2] F. D. Becchetti, Jr., and G. W. Greenlees, Phys. Rev. **182**, 1190 (1969).

II. MODEL

A. Formulation

In computing the interaction potential between an incident nucleon and the target nucleus, it was assumed in Ref. 1 that the effective potentials arising from target polarization and antisymmetrization effects are small and can be neglected. These assumptions are probably reasonable since the fairly strong absorptive component in the optical potential ensures that the elastic scattering is sensitive primarily to the surface region where it has been shown that these effects have small magnitudes.[3]

The nucleon-nucleon potential was taken to have the form

$$u_{0i}=u_d(r_{0i})+u_\tau(r_{0i})\boldsymbol{\tau}_0\cdot\boldsymbol{\tau}_i+u_\sigma(r_{0i})\boldsymbol{\sigma}_0\cdot\boldsymbol{\sigma}_i$$
$$+u_{\sigma\tau}(r_{0i})\boldsymbol{\sigma}_0\cdot\boldsymbol{\sigma}_i\boldsymbol{\tau}_0\cdot\boldsymbol{\tau}_i+[u_t(r_{0i})+u_{t\tau}\boldsymbol{\tau}_0\cdot\boldsymbol{\tau}_i]S_{12}$$
$$+u_{ls}(r_{0i})\,(1/\hbar)[(\mathbf{r}_0-\mathbf{r}_i)\times(\mathbf{p}_0-\mathbf{p}_i)\cdot(\boldsymbol{\sigma}_0+\boldsymbol{\sigma}_i)], \quad \cdots \tag{1}$$

where S_{12} is the tensor force operator. For nuclei with total angular momentum zero, the contributions to the real effective interaction potential U_0 come from the first, second, and last terms of Eq. (1). Hence,

$$U_0=U_R+U_S+U_{so}, \tag{2}$$

where

$$U_R=\int[\rho_n(\mathbf{r})+\rho_p(\mathbf{r})]u_d(|\mathbf{r}-\mathbf{r}_0|)\,d\mathbf{r}, \tag{3}$$

$$U_S=\left(\int[\rho_p(\mathbf{r})-\rho_n(\mathbf{r})]u_\tau(|\mathbf{r}-\mathbf{r}_0|)\,d\mathbf{r}\right)\tau_{0z}, \tag{4}$$

$$U_{so}=\left[-\hbar^{-1}\sum_{n=1}^{\infty}\frac{4\pi}{(2n+1)!}\frac{2n}{r_0}\frac{d}{dr_0}\left(\frac{2(n-1)}{r_0}\frac{d^{2n-3}}{dr_0^{2n-3}}\rho_m\right.\right.$$
$$\left.\left.+\frac{d^{2n-2}}{dr_0^{2n-2}}\rho_m\right)\times\int_0^\infty u_{ls}(\eta)\eta^{2n+2}d\eta\right]\mathbf{l}_0\cdot\boldsymbol{\sigma}_0, \tag{5}$$

with

$$\tau_{0z}=+1 \quad \text{for protons,}$$
$$\tau_{0z}=-1 \quad \text{for neutrons.}$$

The right-hand side of Eq. (5) is an asymptotic series and care must be taken in its summation.[4]

Also,

$$\rho_m(\mathbf{r})=\rho_n(\mathbf{r})+\rho_p(\mathbf{r}), \tag{6}$$

where ρ_p, ρ_n, and ρ_m are the proton, neutron, and matter distributions of the target nucleus.

The existence of open reaction channels is taken into account by adding a phenomenological imaginary potential to U_0, resulting in a complex potential of the type commonly used to analyze data on the scattering of nucleons by complex nuclei.

B. Application

It is clear from Eqs. (3)–(5) that choosing specific forms for ρ_p, ρ_n, u_d, u_τ, and u_{ls} will allow computation of U_R, U_S, and U_{so}. The method followed in this analysis is to assume suitable forms for ρ_p, u_d, u_τ, and u_{ls}, parametrize ρ_n, and search to fit the experimental data. The strength parameters of the folded potentials are left adjustable to allow for small corrections due to effects ignored by the model.

Thus, the procedures followed in obtaining the effective interaction potential are to

(1) assume ρ_n has a Woods-Saxon form with parameters R_n and a_n;
(2) assume ρ_p has a Woods-Saxon form with parameters R_p and a_p derived from electron scattering and muonic x-ray measurements;
(3) assume a form for u_d;
(4) assume $\mu_\tau(r)=-\zeta u_d(r)$;
(5) assume u_{ls} has a Yukawa shape with a mean square radius $\langle r^2\rangle_{ls}$ of 0.5 F^2;
(6) obtain the forms of U_R, U_S, and U_{so} by folding the appropriate quantities in Eqs. (3)–(5), leaving the coefficients as strength parameters;
(7) introduce an imaginary potential with both surface and volume components.

In Ref. 1, a value of $\langle r^2\rangle_d=2.25$ F^2 was chosen for the two-body force range as determined from the fits to the proton-nucleus elastic scattering data. This value is in reasonable agreement with values obtained from phenomenological analyses of α-α scattering, and from a phenomenological nucleon-nucleon potential used in a number of scattering problems involving light nuclei,[5,6] and was taken as the starting value in the present analysis.

An indication of the magnitude of ζ, the ratio of the isospin to the direct part of the nucleon-nucleon potential, can be obtained from the two-body potential of Ref. 6, where a value of 0.48 was used.

A Yukawa form for u_{ls} with a mean square radius of 0.5 F^2 is expected to be satisfactory since the two-body spin-orbit potential is short-ranged, with $\hbar/Mc$ equal to about 0.3 F.[7]

Although the values chosen for $\langle r^2\rangle_d$, $\langle r^2\rangle_{ls}$, and ζ are reasonable in relation to other work, it is, nevertheless, necessary to explore the sensitivity of the model predictions and parameters to these quantities.

The interaction potential used here may be written as

$$U_{op}(r)=U_C(r)-V_{RS}\{I(r)/[I_p(0)+I_n(0)]\}$$
$$-iW_V f_I(r)+iW_S 4a_I[df_I(r)/dr]-V_{so}I_{so}(r)\boldsymbol{\sigma}\cdot\mathbf{l}, \tag{7}$$

[3] S. D. Drell, Phys. Rev. **100**, 97 (1955).
[4] The first term ($n=1$) in Eq. (5) has been derived by R. J. Blin-Stoyle, Phil. Mag. **46**, 973 (1955).
[5] S. Ali and A. R. Bodmer, Nucl. Phys. **80**, 99 (1966).
[6] Y. C. Tang, E. Schmid, and K. Wildermuth, Phys. Rev. **131**, 2631 (1963); S. Okai and S. C. Park, *ibid.* **145**, 787 (1966); D. R. Thompson and Y. C. Tang, *ibid.* **159**, 806 (1967).
[7] R. A. Bryan and B. L. Scott, Phys. Rev. **135**, B434 (1964).

where $U_C(r)$ is the Coulomb potential between a nucleon and the appropriate Woods-Saxon charge distribution determined from electron scattering and muonic x-ray measurements.

Also,

$$I(r)=[I_n(r)+I_p(r)]+\zeta[I_n(r)-I_p(r)]\tau_{0z}, \quad (8)$$

$$I_n(r)=\int f_n(\boldsymbol{\eta})f_d(|\boldsymbol{\eta}-\mathbf{r}|)\,d\boldsymbol{\eta}, \quad (9)$$

$$I_p(r)=\int f_p(\boldsymbol{\eta})f_d(|\boldsymbol{\eta}-\mathbf{r}|)\,d\boldsymbol{\eta}, \quad (10)$$

$$f_d(r)=e^{(-\mu r)}/\mu r, \quad (11)$$

$$\rho_n(r)/\rho_{n0}=f_n(r)=\{1+\exp[(r-R_n)/a_n]\}^{-1}, \quad (12)$$

$$\rho_p(r)/\rho_{p0}=f_p(r)=\{1+\exp[(r-R_p)/a_p]\}^{-1}, \quad (13)$$

$$f_I(r)=\{1+\exp[(r-R_I)/a_I]\}^{-1}. \quad (14)$$

With a Yukawa form for $u_{ls}(e^{-\beta r}/\beta r)$, the spin-orbit form factor reduces to

$$I_{so}(r)=2\pi\int_0^\infty G(r,x)\,(\rho_n(x)+\rho_p(x))\,dx, \quad (15)$$

where

$$G(r,x)=\frac{2x^2}{b\beta}\left\{\frac{x}{br}\left[e^{-\beta y}\left(\frac{y^2}{\beta}+\frac{2y}{\beta^2}-\frac{a}{\beta}+\frac{2}{\beta^3}\right)\right]_{(a-b)^{1/2}}^{(a+b)^{1/2}}+\left(\frac{e^{-\beta y}}{\beta}\right)_{(a-b)^{1/2}}^{(a+b)^{1/2}}\right\}$$

and

$$a=r^2+x^2, \qquad b=2rx.$$

It is clear that this formulation requires a separate numerical integration to obtain U_R, U_S, and U_{so}, and thus a rather long computing period for each iteration.

In order to obtain nuclear-proton distributions from nuclear-charge distributions, the following procedures were adopted. Since charge measurements were not available for all the nuclei studied at the time of analysis, interpolated values were taken from the work of Acker *et al.*,[8] in which nuclear-charge distributions are well represented ($A=50$–210) by a Woods-Saxon shape

$$\{1+\exp[(r-R_{ch})/a_{ch}]\}^{-1},$$

with

$$a_{ch}=0.502 \text{ F}$$

and

$$R_{ch}=(1.106+1.05\times10^{-4}A)A^{1/3} \text{ F}.$$

Correcting for the finite size of the proton allows nuclear-proton distributions to be extracted from these charge distributions. The major effect of unfolding the proton size is to reduce the falloff distance of the distribution and leave the half-way radius almost unchanged. Taking the mean square radius of the proton to be 0.64 F^2, and assuming that the proton half-way radius $R_p=R_{ch}$, a_p was obtained from the relation $\langle r^2\rangle_{ch}=\langle r^2\rangle_p+0.64$. Thus $a_p=0.454$ F for all A. Using these proton parameters, the corresponding neutron distributions which gave fits to the data were found.

From Eqs. (3) and (4), with $u_\tau=-\zeta u_d$, it follows that

$$\langle r^2\rangle_R=(N/A)\langle r^2\rangle_n+(Z/A)\langle r^2\rangle_p+\langle r^2\rangle_d, \quad (16)$$

$$\langle r^2\rangle_S=[N/(N-Z)]\langle r^2\rangle_n-[Z/(N-Z)]\langle r^2\rangle_p+\langle r^2\rangle_d, \quad (17)$$

and hence

$$\langle r^2\rangle_{RS}[1+\zeta\tau_{0z}(N-Z)/A]=\langle r^2\rangle_d[1+\zeta\tau_{0z}(N-Z)/A]+\langle r^2\rangle_n(N/A)(1+\zeta\tau_{0z})+\langle r^2\rangle_p(Z/A)(1-\zeta\tau_{0z}), \quad (18)$$

where $\langle r^2\rangle_{RS}$, $\langle r^2\rangle_d$, $\langle r^2\rangle_n$, and $\langle r^2\rangle_p$ are the mean square radii of the real central potential $U_{RS}(=U_R+U_S)$, the spin- and isospin-independent part of the two-body potential u_d, the neutron distribution ρ_n, and the proton distribution ρ_p, respectively.

Also,

$$J_R=AJ_d, \quad (19)$$

$$J_S=(N-Z)\zeta J_d\tau_{0z}, \quad (20)$$

$$J_{RS}/A=J_d\{1+[(N-Z)/A]\zeta\tau_{0z}\}, \quad (21)$$

where

$$J_R=-\int U_R(\eta)\,d\boldsymbol{\eta}, \quad (22)$$

$$J_S=-\int U_S(\eta)\,d\boldsymbol{\eta}, \quad (23)$$

$$J_{RS}=J_R+J_S, \quad (24)$$

and

$$J_d=-\int u_d(\eta)\,d\boldsymbol{\eta} \quad (25)$$

are the volume integrals of the potentials involved.

Note that Eqs. (16) to (21) are analytic and independent of the forms of ρ and u and hence of the potential forms used. In particular, these expressions are independent of the shape of the symmetry potential U_S.

III. ANALYSIS OF DATA

The performance of the model has been tested by analyzing proton elastic scattering data at 30.3 MeV. The polarization data used differ from those used in the earlier analysis.[1] Since that analysis was completed, large-angle polarization data for ^{58}Ni, ^{60}Ni, and ^{208}Pb and forward-angle data for ^{56}Fe have become available at energies close to 30.3 MeV.[9] The earlier polarization data, used in Ref. 1, was for a proton energy of 29.0 MeV and presented some difficulties in analysis and

[8] H. A. Acker, G. Backenstoss, C. Daum, J. C. Sens, and S. A. Dewitt, Nucl. Phys. **87**, 1 (1966).

[9] D. L. Watson, J. Lowe, J. C. Dore, R. M. Craig, and D. J. Baugh, Nucl. Phys. **A92**, 193 (1967); J. Lowe (private communication).

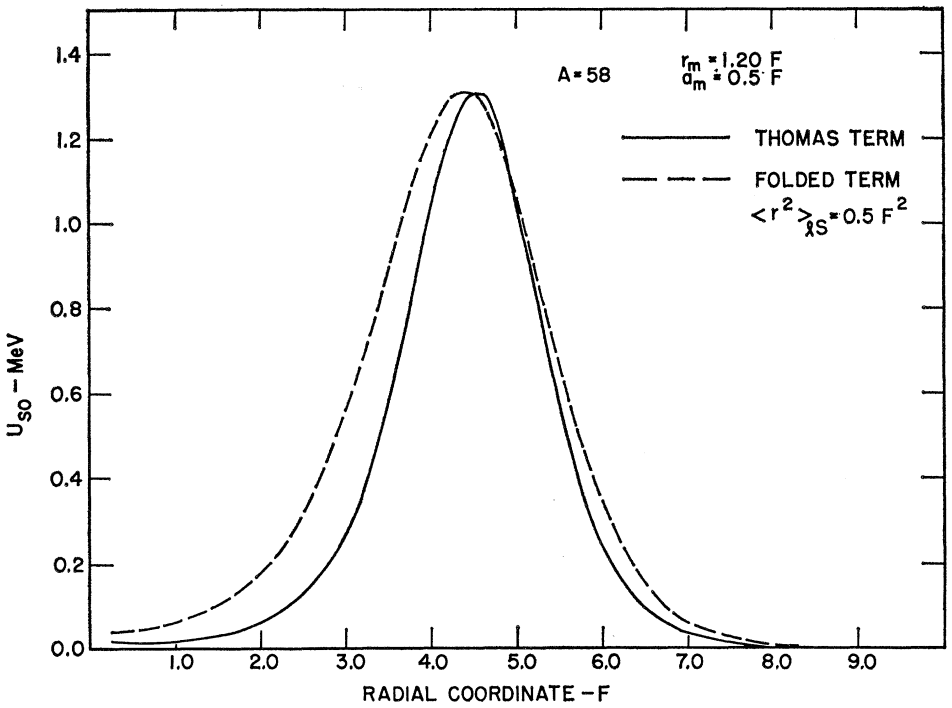

FIG. 1. Plot of spin-orbit potentials obtained from the first term ($n=1$) of Eq. (5) corresponding to a zero range for u_{ls} and all the terms with $\langle r^2 \rangle_{ls}=0.5$ F^2. The calculation was done for $A=58$, $r_m=1.2$ F, and $a_m=0.5$ F, using the model developed in Ref. 1. The potentials have been normalized at their maximum value.

interpretation. In the present analysis, only the new polarization data[9] is used.

The model, as developed, has four strength parameters V_{RS}, W_V, W_S, and V_{so} and four geometrical parameters R_n, a_n, R_I, and a_I. These parameters were varied using a search procedure to find a minimum in χ^2, defined by

$$\chi^2=N^{-1}\sum_{i=1}^{N}\left(\frac{q_{\text{theor}}(\theta_i)-q_{\text{expt}}(\theta_i)}{q_{\text{error}}(\theta_i)}\right)^2,$$

where $q_{\text{theor}}(\theta_i)$ and $q_{\text{expt}}(\theta_i)$ are the theoretical and experimental quantities at scattering angle θ_i, respectively, and $q_{\text{error}}(\theta_i)$ is the associated experimental error. In the search routine used to minimize χ^2, the model predictions for polarization were averaged over the experimental angular acceptance before comparison was made with the data.

Differential cross-section data on ^{56}Fe, ^{58}Ni, ^{59}Co, ^{60}Ni, ^{120}Sn, and ^{208}Pb[10] and polarization data on ^{56}Fe, ^{58}Ni, ^{60}Ni, and ^{208}Pb[9] were used in the analysis. The cross-section data, in general, cover an angular range of 4° to 160° in 2° intervals and have an accuracy of 1 to 4% except for a few forward and backward angles. The polarization data spans the angular range 20° to 120° for ^{56}Fe and 100° to 160° for ^{58}Ni, ^{60}Ni, and ^{208}Pb in 5° intervals with an absolute accuracy of 0.03 to 0.13.

Although it was in general possible to search on all eight parameters simultaneously and obtain a converged minimum in χ^2, the searches could be done most efficiently by considering three groups of parameters. These groups were (1) V_{RS}, W_V, W_S, R_n, and R_I; (2) V_{RS}, W_V, W_S, a_n, a_I; and (3) V_{RS}, W_V, W_S, V_{so}, R_n, R_I, a_n, a_I. Since the rms radii are well defined compared to individual radii and diffuseness param-

TABLE I. Values of $\langle r^2 \rangle_m^{1/2}$ obtained from best-fit parameter sets for the approximate spin-orbit term ($n=1$) and for the full spin-orbit term with $\langle r^2 \rangle_{ls}=0.5$ F^2. In both cases, the matter parametrization of Ref. 1 was used with $\langle r^2 \rangle_d=2.25$ F^2 (Yukawa).

Element	$\langle r^2 \rangle_{ls}$ (F^2)	$\langle r^2 \rangle_m^{1/2}$ (F)	χ_σ^2	χ_P^2	χ_T^2
^{56}Fe	0	4.05	9.8	8.0	9.2
	0.5	4.03	8.0	7.2	7.7
^{58}Ni	0	4.11	5.3	10.9	6.7
	0.5	4.07	4.3	9.0	5.5
^{59}Co	0	4.10	4.9	...	4.9
	0.5	4.08	3.9	...	3.9
^{60}Ni	0	4.16	4.1	9.6	5.4
	0.5	4.13	3.3	7.0	4.2
^{120}Sn	0	5.17	6.2	...	6.2
	0.5	5.14	6.0	...	6.0
^{208}Pb	0	5.82	1.3	2.9	1.8
	0.5	5.86	1.1	2.4	1.5

[10] B. W. Ridley and J. F. Turner, Nucl. Phys. 58, 497 (1964).

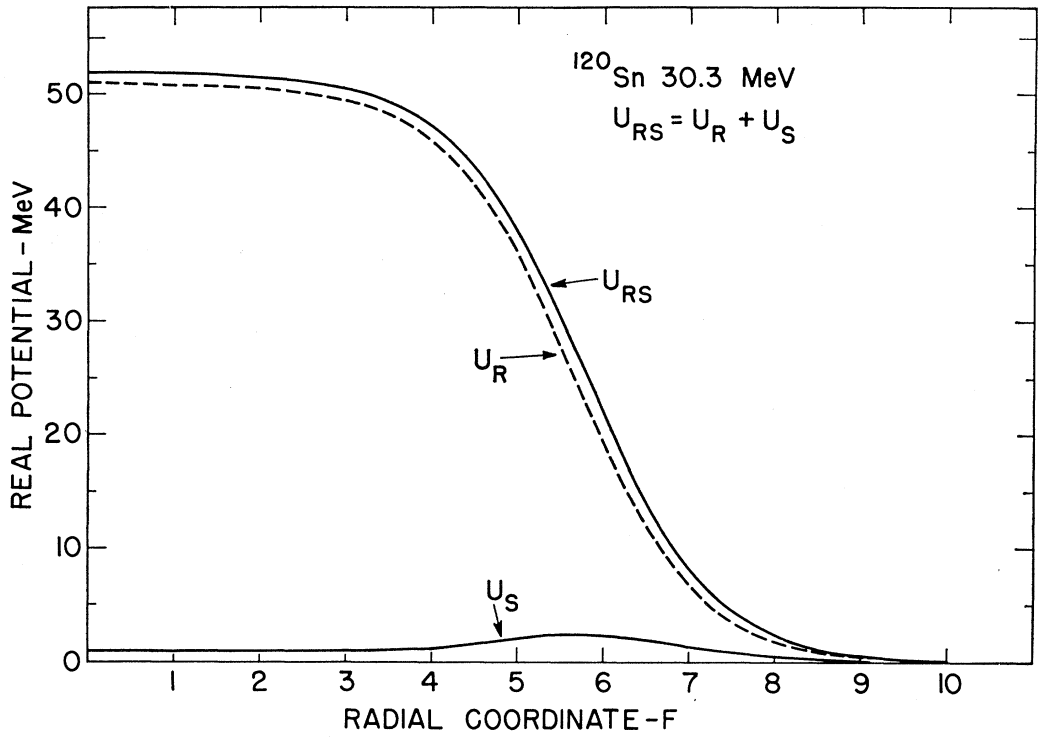

FIG 2. Plot of the direct (U_R) and isosopin (U_S) contributions to the real central potential (U_{RS}) for ^{120}Sn at 30.3 MeV using the full model outlined in Sec. II with Yukawa forms, $\langle r^2\rangle_d=2.25$ F^2, $\langle r^2\rangle_{ls}=0.5$ F^2, and $\zeta=0.48$.

eters, searches (1) and (2) consider the two sets of geometrical parameters separately. Also, since the cross section is not very sensitive to the magnitude of the spin-orbit potential V_{so}, this parameter is not searched upon until a reasonable optimum χ^2 fit has been obtained.

A. Spin-Orbit Folding

The analysis of Ref. 1 used only the first term ($n=1$) of Eq. (5) in calculating the spin-orbit potential. This corresponds to zero range for u_{ls} and is similar to the usual Thomas derivative term. Figure 1 compares the spin-orbit potential obtained from the first term with the potential obtained from the full folding including all terms and assuming a Yukawa two-body spin-orbit force with a mean square radius of 0.5 F^2. The similarity of the two curves of Fig. 1 confirms that the first term of the series [Eq. (5)] is dominant as was anticipated in Ref. 1. The short range of the two-body spin-orbit force[7] ensures that terms with $n>1$ have a rapid variation with r_0 for any reasonable form for ρ_m and hence give only a small net contribution. The major effect of the full folding is to extend the tail of the distribution beyond that given by the first term. In order to maintain the same tail with the full folding, as was obtained using only the first term, the matter and therefore the neutron rms radii will need to be reduced somewhat.

The changes in $\langle r^2\rangle_m^{1/2}$ which take place with the full-spin-orbit folding are shown in Table I, in which best-fit parameters were obtained using the matter parameterization of Ref. 1 for the approximate spin-orbit term ($n=1$) and for the full spin-orbit term with $\langle r^2\rangle_{ls}=0.5$ F^2. Although the fits to the data, as measured by χ^2, are not significantly changed, the general result of including all the contributions to the spin-orbit potential is to decrease $\langle r^2\rangle_m^{1/2}$ by about 0.03 F and $\langle r^2\rangle_n^{1/2}$ by about 0.06 F.

B. Full Symmetry Folding

In Ref. 1, it was assumed that $\rho_p/\rho_n=Z/N$ for all r giving the isospin term a volume form; this allowed the term to be implicitly included as part of the real central potential through an adjustment of its strength parameter. However, the results obtained indicated that the neutron density distributions extend beyond the proton distributions so that, in fact, the isospin term should be surface-peaked. This inconsistency is removed if the isospin term is calculated from Eq. (4). In order to do this, the same form and range is assumed for the two-body isospin term u_τ and the direct term u_d with a relative strength $\zeta(=-u_\tau/u_d)$. A value for ζ of 0.48 was taken as discussed in Sec. II B. The effect of using a surface-peaked rather than a volume isospin term may be examined by fitting the data with the complete model, as outlined in Sec. II, for $\zeta=0$ and

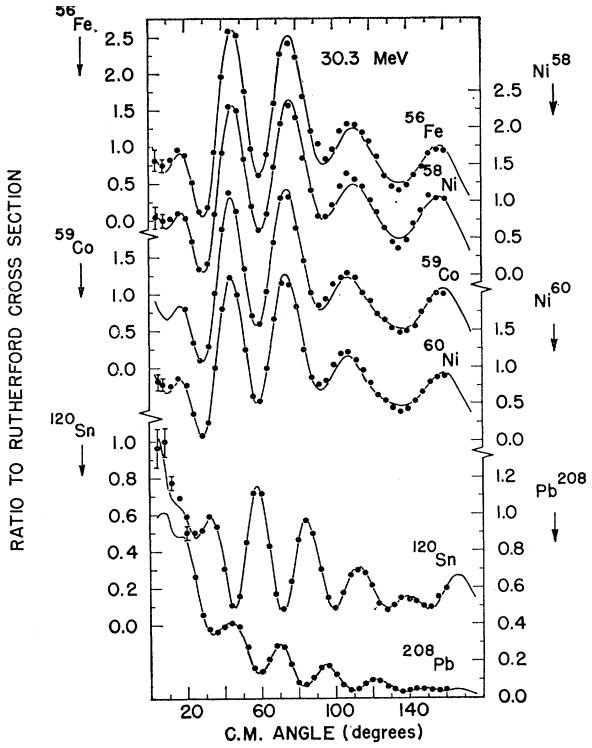

FIG. 3. Fits to the 30.3-MeV cross-section data for various nuclei. Solid lines are the model predictions; the points are the data of Ridley and Turner (Ref. 10). Where error bars are not shown, they are less than the size of the points.

for $\zeta=0.48$. The values for $\langle r^2\rangle_m^{1/2}$ obtained in this way are given in Table II for the 30.3-MeV data; these were obtained from best-fit parameters using $\langle r^2\rangle_d=2.25$ F^2 and $\langle r^2\rangle_{ls}=0.5$ F^2. Table II shows that $\langle r^2\rangle_m^{1/2}$ is decreased by about 0.1 F when the full isospin term is included, and that the χ^2 values are slightly

TABLE II. Values of $\langle r^2\rangle_m^{1/2}$ for the 30.3-MeV data obtained from best-fit parameter sets using the complete model outlined in Sec. II for $\zeta=0$ and $\zeta=0.48$ with Yukawa forms, $\langle r^2\rangle_d=2.25$ F^2, and $\langle r^2\rangle_{ls}=0.5$ F.

Element	ζ	$\langle r^2\rangle_m^{1/2}$ (F)	χ_σ^2	χ_p^2	χ_T^2
^{56}Fe	0	4.06	9.3	8.0	8.9
	0.48	3.95	9.1	7.2	8.5
^{58}Ni	0	4.14	4.8	9.5	6.0
	0.48	4.00	4.7	8.8	5.7
^{59}Co	0	4.09	4.9	...	4.9
	0.48	3.99	4.7	...	4.7
^{60}Ni	0	4.16	3.8	7.8	4.8
	0.48	4.04	3.7	7.2	4.6
^{120}Sn	0	4.98	2.3	...	2.3
	0.48	4.88	2.3	...	2.3
^{208}Pb	0	5.83	1.1	2.4	1.5
	0.48	5.73	1.4	2.7	1.8

improved in most cases. This change corresponds to an adjustment of the matter parameters with the addition of a surface-peaked isospin term to maintain as far as possible an optimum form for the real central potential. This is illustrated in Fig. 2 which shows the direct and isospin contributions to the real central potential. Their sum is indistinguishable from the real

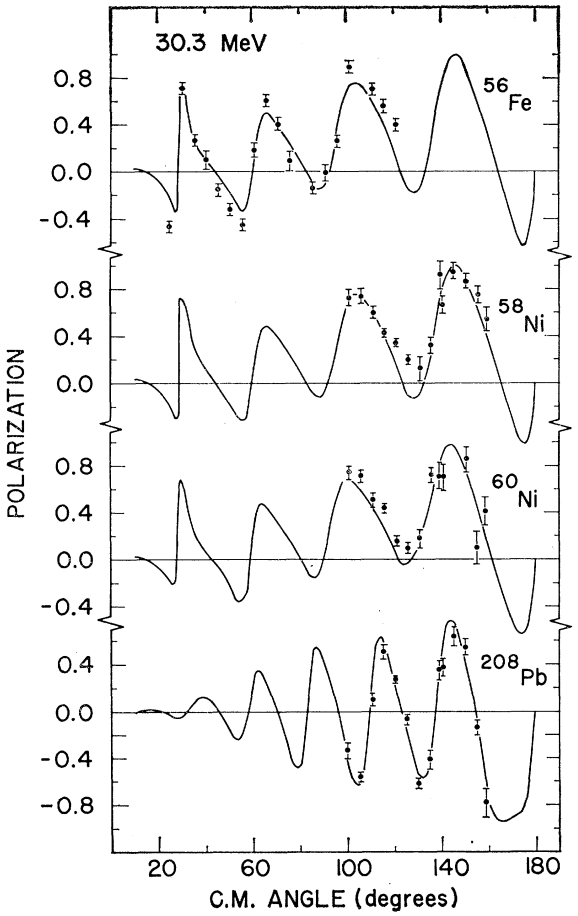

FIG. 4. Fits to the 30.3-MeV polarization data for various nuclei. Solid lines are the model predictions; the points are the data of Watson *et al.* (Ref. 9).

central potential obtained using the matter parametrization of Ref. 1, with $\langle r^2\rangle_{ls}=0.5$ F^2 in both cases.

C. Best Fits Using Yukawa Two-Body Potentials

Table III gives the best-fit parameter sets obtained for the 30.3-MeV cross section and polarization data using the complete model with Yukawa forms for the direct (2.25 F^2) and spin-orbit (0.5 F^2) terms. The quality of fits as measured by the χ_σ^2 values is generally better than obtained in Ref. 1. Of course, χ_p^2 is not directly comparable since the polarization data are different. The normalization used for the full spin-orbit term is different from the usual Thomas term. A strength of about 2000 MeV in Table III corresponds

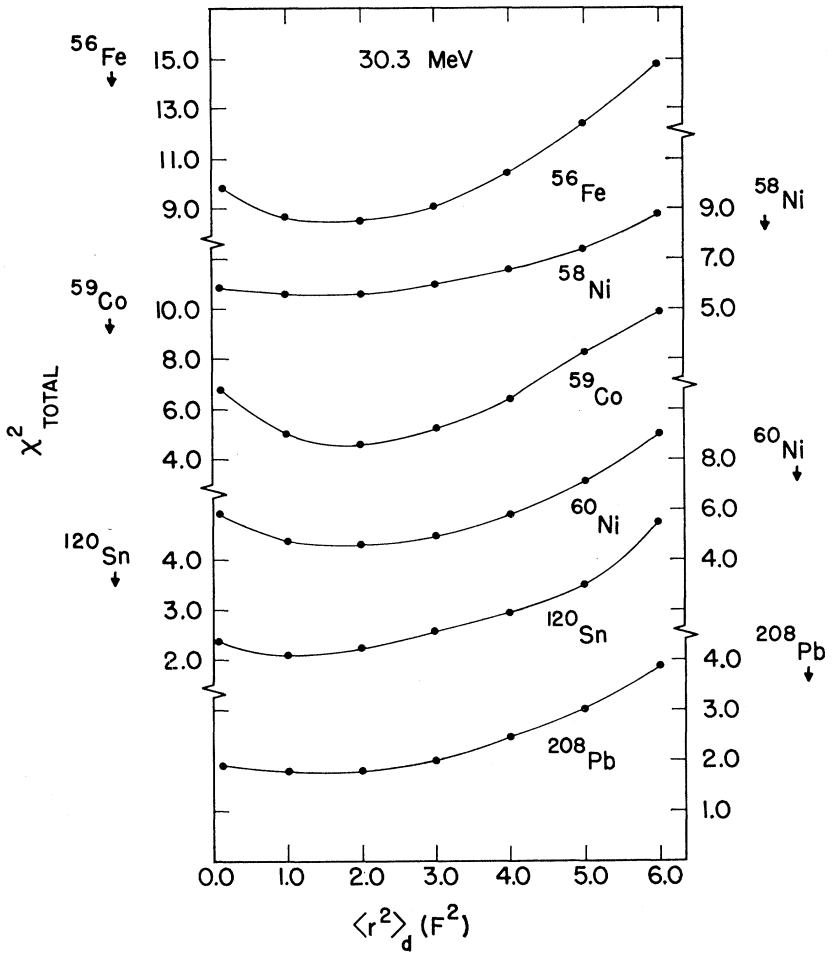

FIG. 5. Variation of best-fit χ^2 values for elastic proton scattering data at 30.3 MeV with Yukawa two-body-force range $\langle r^2 \rangle_d$, using $\langle r^2 \rangle_{ls}=0.5$ F^2 and $\zeta=0.48$.

to a strength of 6 MeV in the usual formulation. Comparison of the experimental data and model predictions are given in Figs. 3 and 4.

IV. DEPENDENCE ON NUCLEON-NUCLEON PARAMETERS

A. Sensitivity to the Yukawa Two-Body-Force Range

In the analysis presented so far the direct part of the nucleon-nucleon force has been taken to have a Yukawa shape with a range of 2.25 F^2 as indicated from Ref. 1. In order to explore the sensitivity of the model predictions to this range, the analysis was repeated for a number of values for $\langle r^2 \rangle_d$ between 0.1 and 6.0 F^2 with $\zeta=0.48$ and $\langle r^2 \rangle_{ls}=0.5$ F^2. The parameters found for ^{208}Pb at 30.3 MeV are given in Table IV and plots of χ^2 versus $\langle r^2 \rangle_d$ for all cases are given in Fig. 5. Systematic trends in the parameters for variations in $\langle r^2 \rangle_d$ are exhibited in Table IV; in particular, a decrease in $\langle r^2 \rangle_n^{1/2}$ with increasing $\langle r^2 \rangle_d$ is evident. However, the rms radius of the folded real central potential $\langle r^2 \rangle_{RS}^{1/2}$, is quite constant over the region of acceptable χ^2. The criterion for an acceptable fit is the same as in Ref. 1, where it was found that the fits became visibly worse when χ^2 increased from its optimum value by a factor of 1.5 for medium-weight nuclei, and by a factor of 2.0 for heavy-weight nuclei. In Table IV, the neutron parameters are adjusting for variations in $\langle r^2 \rangle_d$ so as to maintain the real central potential close to the optimum shape.

In Fig. 5, it is clear that the fits to the data are not significantly restricting the choice of $\langle r^2 \rangle_d$ value. The situation differs from the findings of Ref. 1, where a choice for $\langle r^2 \rangle_d$ of 2.25 F^2 was made.[11] In the present case it is not possible to draw any conclusions concerning the appropriate value of $\langle r^2 \rangle_d$.

B. Sensitivity to the Magnitude of the Isospin Term

In Sec. II, a value of $\zeta=0.48$ was chosen from published analyses of nucleon-nucleon data. In order to test the sensitivity of the fits to the magnitude of the

[11] The minima around 2.25 F^2 found in Ref. 1 were due in large part to a rise in the χ^2 values for small values of $\langle r^2 \rangle_d$. This rise was due to inaccuracies in the numerical integration technique when $\langle r^2 \rangle_d$ was small. These inaccuracies have been removed in the present work.

TABLE III. Best-fit parameter sets for the 30.3-MeV data using Yukawa forms with $\langle r^2\rangle_d = 2.25$ F^2, $\langle r^2\rangle_{ls} = 0.5$ F^2, and $\zeta = 0.48$.

	Element					
	^{56}Fe	^{58}Ni	^{59}Co	^{60}Ni	^{120}Sn	^{208}Pb
V_{RS} (MeV)	53.37	55.07	53.95	53.81	50.96	52.01
W_V (MeV)	3.57	4.18	3.34	3.55	2.77	1.53
W_S (MeV)	4.84	4.01	4.92	4.78	7.37	9.81
r_I (F)	1.330	1.355	1.311	1.318	1.316	1.244
a_I (F)	0.582	0.526	0.621	0.605	0.640	0.738
V_{so} (MeV)	1611.6	1597.6	1649.0	1577.7	1705.3	1659.1
r_n (F)	1.166	1.145	1.157	1.170	1.214	1.212
a_n (F)	0.619	0.670	0.619	0.631	0.555	0.529
$\langle r^2\rangle_n^{1/2}$ (F)	4.15	4.24	4.18	4.26	5.08	5.90
$\langle r^2\rangle_{RS}^{1/2}$ (F)	4.32	4.39	4.35	4.38	5.21	6.01
J_{RS}/A (MeV F^3)	400.6	400.1	401.6	403.0	398.8	408.1
χ_σ^2	9.1	4.7	4.7	3.7	2.3	1.4
χ_p^2	7.2	8.8	...	7.2	...	2.7
χ_T^2	8.5	5.7	4.7	4.6	2.3	1.8

TABLE IV. Best-fit parameter sets found in the analysis of 30.3-MeV differential elastic scattering data for ^{208}Pb using various values of $\langle r^2\rangle_d$ and a Yukawa form.

	$\langle r^2\rangle_d$ (F^2)						
	0.1	1.0	2.0	3.0	4.0	5.0	6.0
V_{RS} (MeV)	51.21	51.56	51.87	52.63	53.45	54.07	54.33
W_V (MeV)	1.94	1.53	1.49	1.72	2.18	2.38	2.48
W_S (MeV)	8.84	9.51	9.81	9.67	9.02	8.84	9.06
r_I (F)	1.243	1.239	1.241	1.260	1.286	1.310	1.320
a_I (F)	0.742	0.746	0.740	0.734	0.731	0.714	0.686
V_{so} (F)	1663.0	1676.5	1670.7	1591.6	1506.2	1445.5	1364.3
r_n (F)	1.213	1.211	1.214	1.202	1.188	1.177	1.179
a_n (F)	0.673	0.621	0.546	0.489	0.411	0.330	0.181
$\langle r^2\rangle_n^{1/2}$ (F)	6.11	6.02	5.93	5.81	5.66	5.54	5.45
$\langle r^2\rangle_{RS}^{1/2}$ (F)	6.00	6.00	6.01	6.00	5.97	5.96	5.97
J_{RS}/A (MeV F^3)	411.0	409.9	410.3	407.9	403.7	400.5	401.6
χ_σ^2	1.3	1.3	1.4	1.6	1.9	2.3	2.7
χ_p^2	3.4	2.9	2.6	3.1	3.7	4.9	6.7
χ_T^2	1.9	1.7	1.7	2.0	2.4	3.0	3.9

TABLE V. Best-fit parameter sets found in the analysis of 30.3-MeV differential elastic scattering data for ^{120}Sn using various values of ζ.

	ζ				
	−1.0	−0.5	0.0	0.5	1.0
V_{RS} (MeV)	41.93	49.86	52.04	50.88	48.66
W_V (MeV)	2.83	2.41	2.66	2.79	2.90
W_S (MeV)	6.48	8.03	7.63	7.33	7.11
r_I (F)	1.323	1.300	1.313	1.316	1.319
a_I (F)	0.728	0.639	0.636	0.640	0.644
V_{so} (F)	2119.2	2205.6	1836.3	1700.2	1634.5
r_n (F)	1.648	1.375	1.259	1.213	1.191
a_n (F)	0.122	0.512	0.555	0.555	0.547
$\langle r^2\rangle_n^{1/2}$ (F)	6.31	5.59	5.24	5.07	4.98
$\langle r^2\rangle_{RS}^{1/2}$ (F)	4.83	5.16	5.20	5.21	5.20
J_{RS}/A (MeV F^3)	358.4	390.3	397.3	398.8	399.2
χ^2	6.1	2.2	2.3	2.3	2.3

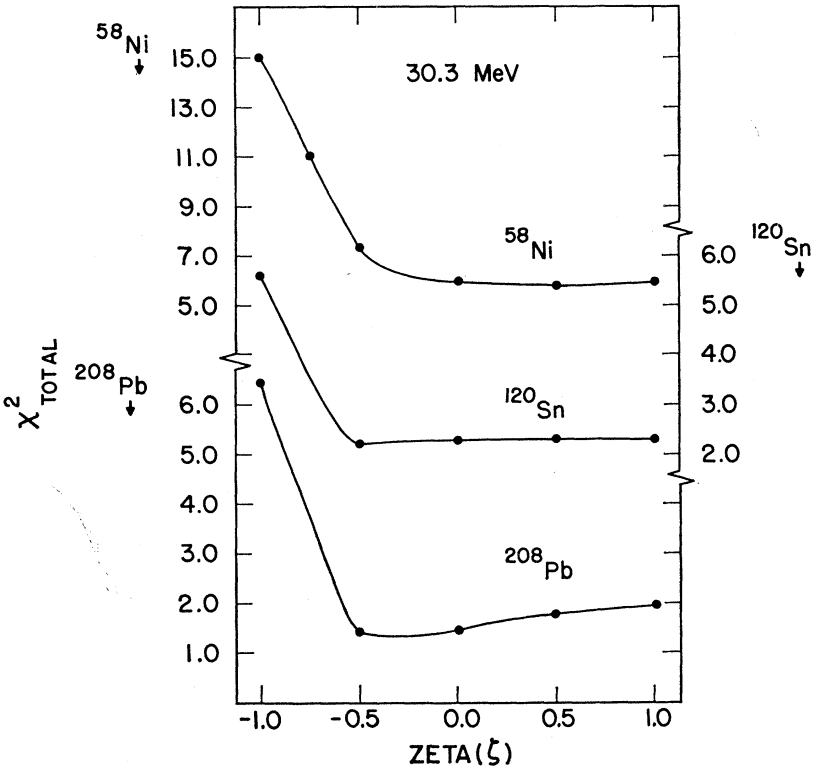

FIG. 6. Variation of best-fit χ^2 values for ^{58}Ni, ^{120}Sn, and ^{208}Pb at 30.3 MeV with ζ, using Yukawa forms, $\langle r^2\rangle_d=2.25$ F^2, and $\langle r^2\rangle_{ls}=0.5$ F^2.

surface-peaked isospin term, best-fit parameter sets were obtained for a variety of nuclei for ζ values between -1.0 and 1.0 with $\langle r^2\rangle_d=2.25$ F^2 and $\langle r^2\rangle_{ls}=0.5$ F^2. A plot of ζ versus χ^2 for ^{58}Ni, ^{120}Sn, and ^{208}Pb at 30.3 MeV is shown in Fig. 6. The curves, typical of all the cases investigated, indicate that any value between $\zeta=-0.5$ and $\zeta=1.0$ will give acceptable fits to the data. This is in agreement with Ref. 1, where acceptable values of ζ were estimated using Eq. (21) and making a straight-line fit to plots of J_{RS}/A versus $(N-Z)/A$. The detailed variation of the parameters for ^{120}Sn is shown in Table V. For acceptable values of χ^2, the neutron geometrical parameters are varying so as to maintain $\langle r^2\rangle_{RS}^{1/2}$, the rms radius of the real central potential, essentially constant.

C. Gaussian Two-Body Force

The insensitivity of the predictions to the parameters chosen for the two-body force (Secs. IV A and IV B) suggests that these parameters should be obtained from the fitting of low-energy nucleon-nucleon scattering data. It is well known that reasonable fits to such data can be obtained with a variety of functional forms. The appropriate choice for the present problem is suggested from the following considerations. In the original formulation of the model in Ref. 1, a variational principle was used with a trial wave function of the form

$$\Psi=\psi(\xi)\phi(r_0, s_0, t_0)F,$$

where ψ is a normalized wave function describing the ground state of the target nucleus, ϕ is the scattering function, and the short-range correlation function F $[=\prod_{i=1}^{A}(r_{0i})]$ was taken as being unity for all r_{0i} values. This assumption concerning F suggests that potentials which vary rapidly at small distances, such as a Yukawa, are not too appropriate in the present context. The forms normally used in fitting low-energy nucleon-nucleon data are the exponential, the Yukawa, and the Gaussian. Of these, the Gaussian is most suitable for use here because of its relatively slow variation at small distances.

Recently, Tang[12] has analyzed low-energy n-p and p-p data using Gaussian singlet and triplet potentials. These potentials reproduce the experimental scattering lengths and give good agreement with the $^1S_0$ phase shifts up to energies around 100 MeV(lab). The volume integrals and mean square radii for the triplet and singlet potentials were 1393 and 1025 MeV F^3 and 3.62 and 5.15 F^2, respectively. The present model uses only a single form for the two-body potential with the range fixed and the strength adjustable so that an appropriate mean of the Tang singlet and triplet ranges must be chosen. This was done by taking the mean of the two mean square radii weighted by the corresponding volume integrals. This yields a mean square radius of 4.27 F^2 for the Gaussian potential to be used for u_d and u_τ in Eqs. (3) and (4). The ratio of strengths

[12] Y. C. Tang (private communication).

TABLE VI. Best-fit parameter sets for 30.3-MeV proton data using a Gaussian for u_d and $\langle r^2\rangle_d = 4.27$ F^2, a Yukawa for u_{ls} and $\langle r^2\rangle_{ls} = 0.5$ F^2, and $\zeta = 0.48$.

	Element					
	^{56}Fe	^{58}Ni	^{59}Co	^{60}Ni	^{120}Sn	^{208}Pb
V_{RS} (MeV)	56.84	57.15	55.21	55.32	51.26	53.65
W_V (MeV)	3.97	4.52	4.22	4.38	4.15	2.12
W_S (MeV)	3.48	3.11	3.23	3.26	4.86	8.79
r_I (F)	1.414	1.381	1.400	1.381	1.344	1.282
a_I (F)	0.601	0.559	0.626	0.621	0.711	0.781
V_{so} (MeV)	1406.7	1392.5	1450.1	1390.7	1440.3	1450.6
r_n (F)	1.093	1.129	1.143	1.154	1.226	1.173
a_n (F)	0.458	0.432	0.378	0.401	0.186	0.383
$\langle r^2\rangle_n^{1/2}$ (F)	3.66	3.75	3.72	3.80	4.74	5.57
$\langle r^2\rangle_{RS}^{1/2}$ (F)	4.21	4.28	4.26	4.32	5.14	5.92
J_{RS}/A (MeV F^3)	379.3	386.1	383.5	387.3	391.7	394.9
χ_σ^2	8.3	8.2	4.0	5.3	2.7	1.4
χ_p^2	9.8	15.7	...	13.3	...	2.7
χ_T^2	8.8	10.2	4.0	7.3	2.7	1.8

($\zeta = -u_\tau/u_d$) was taken as 0.48 as before, and u_{ls} was left unchanged. The best-fit parameters obtained in this way are given in Table VI. The most significant change noticeable in Table VI when compared to Table III, which corresponds to using a Yukawa with mean square radius of 2.25 F^2 for u_d, is a reduction in magnitude of the neutron parameters. The visual quality of the fits is the same in both cases.

V. RESULTS AND DISCUSSION

A. Real Central Potential

It has been shown that the quality of the fit obtained for proton elastic scattering data at 30.3 MeV is insensitive to the details of the potential used. Evidence for this is given in Tables I and II where the effects of removing the approximations of Ref. 1 are shown, in Table IV where the effect of varying $\langle r^2\rangle_d$ is shown, and in Table V where the effect of varying the isospin term is shown. The variations examined in Tables I, II, IV, and V make considerable changes in the real central potential shape in the surface region. However, both the volume integral J_{RS} and the rms radius of the real central potential, $\langle r^2\rangle_{RS}^{1/2}$, remain relatively constant with these changes of shape. This is illustrated in Tables IV and V. The constancy of J_{RS} and $\langle r^2\rangle_{RS}^{1/2}$ is independent of the details of the model used to analyze the data and a summary of values divided by A, obtained here and elsewhere in analyses of the 30.3-MeV data, is given in Table VII. Since the real central potential normally used to fit elastic data contains at least three parameters and only two quantities are well-defined by elastic scattering data, there is an inherent ambiguity present in analyses of such data.

The above discussion applies to the analysis of data from one element at one energy. Examination of the variation of J_{RS} and $\langle r^2\rangle_{RS}^{1/2}$ for a range of elements at the same energy can, in principle, reveal further information. In particular, an increase of the volume integral per particle, for incident protons, would be expected as the neutron-proton ratio of the nucleus increases because of the stronger S-state interaction of

TABLE VII. Values of J_{RS}/A and $\langle r^2\rangle_{RS}^{1/2}$ obtained in different analyses of 30.3-MeV proton elastic scattering data. Typical errors are ±15 MeV F^3 and ±0.15 F.

Element \ Source	J_{RS}/A (MeV F^3)							$\langle r^2\rangle_{RS}^{1/2}$ (F)						
	a	b	c	d	e	f	g	a	b	c	d	e	f	g
^{56}Fe	401	401	408	407	379	...	...	4.32	4.33	4.39	4.39	4.21	...	...
^{58}Ni	400	402	408	406	386	409	395	4.39	4.40	4.46	4.43	4.28	4.38	4.35
^{59}Co	402	403	411	409	384	411	398	4.35	4.35	4.39	4.42	4.26	4.37	4.36
^{60}Ni	403	404	413	409	387	413	396	4.38	4.42	4.46	4.47	4.32	4.42	4.34
^{120}Sn	399	397	402	399	392	406	399	5.21	5.20	5.22	5.23	5.14	5.24	5.21
^{208}Pb	408	411	411	402	395	411	399	6.01	6.02	6.00	5.97	5.92	6.03	5.95

[a] Present work using $V\langle r^2\rangle_d = 2.25$ F^2, $V\langle r^2\rangle_{ls} = 0.5$ F^2, and $\zeta = 0.48$ (Table III).
[b] Present work using $V\langle r^2\rangle_d = 2.25$ F^2, $V\langle r^2\rangle_{ls} = 0.5$ F^2, and $\zeta = 0$.
[c] Present work using $V\langle r^2\rangle_d = 0.1$ F^2, $V\langle r^2\rangle_{ls} = 0.5$ F^2, and $\zeta = 0.48$.
[d] Present work using $V\langle r^2\rangle_d = 4.27$ F^2, $V\langle r^2\rangle_{ls} = 0.5$ F^2, and $\zeta = 0.48$.
[e] Present work using Gaussian $\langle r^2\rangle_d = 4.27$ F^2, $V\langle r^2\rangle_{ls} = 0.5$ F^2, and $\zeta = 0.48$.
[f] From best-fit parameters of Ref. 1.
[g] From best-fit parameters of Satchler, Nucl. Phys. **A92**, 273 (1967).

TABLE VIII. n-p rms-radii differences (F) obtained in various analyses of 30.3-MeV data.

Element	Ref. 1	Yukawa 2.25 F², $\zeta=0.48$ (Table III)	Yukawa 4.27 F², $\zeta=0.48$	Gaussian 4.27 F², $\zeta=0.48$	Error
^{56}Fe	...	0.45	0.22	−0.04	±0.15
^{58}Ni	0.71	0.50	0.24	0.01	±0.18
^{59}Co	0.64	0.43	0.20	−0.03	±0.16
^{60}Ni	0.70	0.48	0.25	0.03	±0.16
^{120}Sn	0.71	0.49	0.27	0.15	±0.19
^{208}Pb	0.64	0.46	0.19	0.13	±0.25

p-n compared to p-p. In the present formulation this variation with nuclei is given by Eq. (21) which, for protons, reduces to

$$J_{RS}/A=J_d[1+\zeta(N-Z)/A]. \quad (26)$$

This equation is independent of the functional forms of the various components of the potential and it can be applied directly to the volume integrals found for individual nuclei without further assumptions. However, it is clear from Table VII that J_{RS}/A is essentially independent of A [or $(N-Z)/A$], which implies that ζ is zero and that no isospin dependence of the potential is evident. This result is clearly at variance with results of analyses of quasi-elastic scattering to analog states. Indeed, the present formalism has been extended to describe such processes in (p, n) [13] and (He^3, t) [14] reactions and yields values for the volume integral of u_τ corresponding to a ζ value of about 0.4, which is in reasonable agreement with the value of 0.48 obtained from two-body data. No explanation is offered for the absence of an isospin dependence of the potential in elastic scattering; it does, however, suggest that some feature of the p-nucleus interaction is missing from the optical-model description. The isospin dependence of the potential strength often found in optical-model analyses is a direct consequence of the introduction of the additional geometrical assumptions that the radius $R=r_0A^{1/3}$ and the diffuseness $a=$const. This causes the volume of the potential per particle to decrease with A and hence the strength, required for a fit, increases to maintain the volume integral per particle constant.[15]

B. Neutron-Proton Radius Differences

The constancy of the real central rms radius for a wide range of values of the two-body potential parameters results in the values obtained for the neutron rms radius being sensitive to the choice of these parameters (Tables IV and V) since they are interconnected via Eq. (18).

The analysis of Ref. 1 using an approximate form of the present model indicated an optimum choice for the Yukawa two-body mean square radius of 2.25± 0.6 F². In the analysis with the complete model, presented here, a choice can no longer be made so the Gaussian force (mean square radius 4.27 F²) was taken. Such a choice is in agreement with the work of Slanina and McManus,[16] who have compared the nucleon-nucleus potentials to be expected using various forms for the two-body interaction with those obtained from phenomenological analyses of experimental data.

The results of removing the assumptions of Ref. 1 concerning the spin-orbit term and the isospin term are shown in Tables I and II and correspond to reductions of 0.1 to 0.2 F in the neutron rms radii when a Yukawa force of mean square radius 2.25 F² is used. An increase in the range of the Yukawa produces corresponding reductions in the neutron radii (Table IV). When the two-body-force parameters were chosen from analyses of two-body data, a Gaussian form of mean square radius 4.27 F² was taken (Sec. IV C). This resulted (Table VI) in further reductions in the neutron radii from those of Table III, where the complete model was used with a Yukawa of mean square radius 2.25 F². Part of these reductions is due to the increase in range and part is due to the change of shape. The results for the neutron-proton rms-radius differences obtained with the various assumptions are given in Table VIII.

The results of Table VIII indicate that using a Yukawa form for u_d (columns 2, 3, and 4) yields n-p radius differences which are about equal for all the nuclei studied ($A=56$ to 208). Using a Gaussian form, however (column 5), yields differences which increase from around zero for medium-weight nuclei to a value of 0.1–0.2 F for heavy nuclei. This latter trend is more in line with physical expectations than the results obtained with the Yukawa form and reinforces the arguments made in Sec. IV C that the Gaussian is a more appropriate form to use in the present model. These results for the n-p rms-radius differences using the Gaussian form are in agreement with other estimates

[13] C. J. Batty, E. Friedman, and G. W. Greenless, Nucl. Phys. **A127**, 368 (1969).
[14] F. D. Becchetti, Jr. (private communication).
[15] G. W. Greenlees, G. J. Pyle, and Y. C. Tang, Phys. Letters **26B**, 658 (1968).
[16] D. Slanina and H. McManus, Nucl. Phys. **A116**, 271 (1968).

obtained using Coulomb energy differences[17] and pion scattering data,[18] but significantly less than estimates obtained from fitting bound-state energy levels in a single-particle potential.[19]

The relative success of the present model in representing elastic scattering data suggests that a first-order treatment is a good approximation and that the effects of antisymmetrization and core polarization are comparatively small at 30 MeV. It should be pointed out, however, that the elastic data analyzed included very few polarization measurements and that the two-body-force form used had only a single range and did not differentiate between singlet and triplet interactions.

[17] J. A. Nolen, Jr., J. P. Schiffer, and N. Williams, Phys. Letters **27B**, 1 (1968); E. Friedman and B. Mandelbaum Nucl. Phys. **A135**, 472 (1969); F. D. Becchetti, Jr. (private communication); H. A. Bethe and P. J. Siemens, Phys. Letters **27B**, 569 (1968).
[18] E. H. Auerbach, H. M. Qureshi, and M. M. Sternheim, Phys. Rev. Letters **21**, 162 (1968).
[19] E. Rost, Phys. Letters **26B**, 184 (1968); L. R. B. Elton, *ibid.* **26B**, 689 (1968); C. J. Batty and G. W. Greenlees, Nucl. Phys., **A133**, 673 (1969).

ACKNOWLEDGMENTS

We gratefully acknowledge the services of the staff of the University of Minnesota Numerical Analysis Center, who operated the CDC 6600 computer used in this work. We also thank Dr. Y. C. Tang for many useful discussions particularly concerning Sec. IV C.

PHYSICAL REVIEW C VOLUME 1, NUMBER 4 APRIL 1970

Investigation of the States of $2s$-$1d$ Shell Nuclei Based on the Four-Particle–Four-Hole State in ^{16}O†

S. N. TEWARI
Lawrence Radiation Laboratory, University of California, Berkeley, California 94720
AND
G. L. STRUBLE
Lawrence Radiation Laboratory and Department of Chemistry, University of California, Berkeley, California 94720
(Received 13 October 1969)

The four-particle–four-hole state in ^{16}O and the corresponding states in the even-even, $N=Z$ nuclei of the $2s$-$1d$ shell have been investigated in the framework of the Hartree-Fock approximation. Detailed calculations were performed in each case to determine the most stable Hartree-Fock solution. By assuming a simple model, the excitation energies of the band heads were calculated showing that ^{24}Mg is the last nucleus where a state analogous to the four-particle–four-hole state in ^{16}O might be observed. Energy levels have been calculated in ^{16}O, ^{20}Ne, and ^{24}Mg using a basis of good angular-momentum states. A comparison between the predicted and the observed energy spectrum has been shown. In ^{16}O, calculations have been performed both with phenomenological and realistic interactions and the results have been compared. The accuracy of the projected angular-momentum states from the twelve-particle–four-hole solution in ^{24}Mg has been estimated and shows that the projected states in this case are close to the eigenstates. We have demonstrated that one of two 0^+ states observed around 7 MeV in ^{20}Ne is an eight-particle–four-hole state.

I. INTRODUCTION

THE analysis of the experimental results of Carter *et al.*[1] suggests that many of the low-lying positive-parity excited states in ^{16}O may be approximately fitted into rotational bands. This identification is further supported by large $E2$ transitions encountered,[2,3] e.g.,

$$B(E2,\ 2_1^+\rightarrow 0_2^+) = 40e^2f^4$$

and

$$B(E2,\ 4^+{}_1\rightarrow 2^+{}_1) = (117\pm 10)e^2f^4.$$

Although the rotational features in ^{16}O are not as striking as in the case of heavy deformed nuclei of the rare-earth region, the interpretation of its experimental data in terms of a rotating deformed intrinsic state is very tempting.

During the last decade the Hartree-Fock (HF) method has been successfully applied to calculate intrinsic states of the deformed nuclei in the $2s$-$1d$ shell.[4] The application of this method to calculate intrinsic states in ^{16}O therefore seems desirable. A number of HF calculations has already been performed[5,6] in ^{16}O, and an analysis of the results of these calculations leads to the important conclusion that the intrinsic state of the rotational band starting at 6.05 MeV is

† Work performed under the auspices of the U.S. Atomic Energy Commission.
[1] E. B. Carter, G. E. Mitchell, and R. H. Davis, Phys. Rev. **133B**, 1421 (1964); **133B**, 1434 (1964).
[2] S. Gorodetzky, P. Mennarth, W. Benenson, P. Chevallier, and F. Scheibling, J. Phys. **24**, 887 (1963).
[3] J. D. Larson and R. H. Spear, Nucl. Phys. **56**, 497 (1964).
[4] G. Ripka, Advan. Phys. **1**, 183 (1968), and all references mentioned therein.
[5] W. H. Bassichis and G. Ripka, Phys. Letters **15**, 320 (1965).
[6] G. J. Stephenson, Jr., and M. K. Banerjee, Phys. Letters **24B**, 209 (1966); M. K. Banerjee, C. A. Levinson, and G. J. Stephenson, Jr., Phys. Rev. **178**, 1709 (1969).